DREAM Interrupted: Severing MuvB from DREAM's pocket protein in *Caenorhabditis elegans* impairs gene repression but not DREAM chromatin assembly

Paul D. Goetsch[*,†,1] and Susan Strome[†]

[*,1]Department of Biological Sciences, Michigan Technological University, Houghton, MI 49931

[†]Department of Molecular, Cell and Developmental Biology, University of California Santa Cruz, Santa Cruz, CA 95064

24 **Interrupting DREAM complex formation**

25

26 **Keywords**

27 DREAM, pocket protein, MuvB, CRISPR/Cas9 genome editing, transcriptional

28 repression

29

30 Corresponding author:

31 Paul D. Goetsch

32 740 Dow ESE building

33 1400 Townsend Drive

34 Houghton, MI 49931

35 Phone: 906-487-1790

36 Email: pdgoetsc@mtu.edu

37

38

39

40

41

42

43

44

45

46

Abstract

The mammalian pocket protein family, which includes the Retinoblastoma protein (pRb) and Rb-like pocket proteins p107 and p130, regulates entry into and exit from the cell cycle by repressing cell cycle gene expression. Although pRb plays a dominant role in mammalian systems, p107 and p130 represent the ancestral pocket proteins. The Rb-like pocket proteins interact with the highly conserved 5-subunit MuvB complex and an E2F-DP transcription factor heterodimer, forming the DREAM (for Dp, Rb-like, E2F, and MuvB) complex. DREAM complex formation on chromatin culminates in direct repression of target genes mediated by the MuvB subcomplex. Here, we examined how the Rb-like pocket protein contributes to DREAM formation by disrupting the interaction between the sole *Caenorhabditis elegans* pocket protein LIN-35 and the MuvB subunit LIN-52 using CRISPR/Cas9 targeted mutagenesis. Disrupting the LIN-35-MuvB association did not affect DREAM chromatin occupancy but did cause a highly penetrant synthetic multivulval (SynMuv) phenotype, indicating that blocking DREAM assembly impairs MuvB function. Some DREAM target genes became derepressed, indicating that for those genes MuvB chromatin binding alone is not sufficient for gene repression and that direct LIN-35-MuvB association potentiates MuvB's innate repressive activity. In a previous study we showed that in worms lacking LIN-35, E2F-DP and MuvB chromatin occupancy is reduced genome-wide. With LIN-35 present, this study demonstrates that the E2F-DP-LIN-35 interaction promotes E2F-DP's chromatin localization, which we hypothesize supports MuvB chromatin occupancy indirectly through DNA. Altogether, this study highlights how the pocket protein family may recruit

regulatory factors like MuvB to chromatin through E2F-DP to facilitate their transcriptional activity.

Introduction

Members of the mammalian Retinoblastoma (Rb) protein family, pRb, p107, and p130, collectively called pocket proteins, serve key roles in regulating transcription during the cell cycle (CLASSON AND DYSON 2001; CLASSON AND HARLOW 2002; COBRINIK 2005; BURKHART AND SAGE 2008; DICK AND RUBIN 2013). In mammalian cells, pRb interacts with activating E2F-DP transcription factor heterodimers (in mammals, E2F1/2/3-DP1/2), sequestering E2F-DP and preventing E2F-DP-mediated activation of early cell cycle genes (HELIN *et al.* 1992; LEES *et al.* 1993; LIBAN *et al.* 2016). In contrast, the Rb-like proteins p107 and p130 interact with repressive E2F-DPs (in mammals, E2F4/5-DP1/2) and a highly conserved 5-subunit MuvB subcomplex (in mammals, LIN9, LIN37, LIN52, LIN54, and RBAP48), forming the 8-subunit DREAM transcriptional repressor complex (KORENJAK *et al.* 2004; LEWIS *et al.* 2004; HARRISON *et al.* 2006; LITOVCHICK *et al.* 2007; SCHMIT *et al.* 2007). When associated with the DREAM complex, MuvB mediates transcriptional repression of early and late cell cycle genes (LITOVCHICK *et al.* 2007; GOETSCH *et al.* 2017; MULLER *et al.* 2017). DREAM functionally overlaps with pRb to repress cell cycle gene expression during cellular quiescence (G_0) (HURFORD *et al.* 1997; LITOVCHICK *et al.* 2007; MULLER *et al.* 2017). Upon progression into the cell cycle, pRb and the Rb-like pocket proteins are phosphorylated by CDK4/6-cyclin D, releasing their respective interaction partners and triggering activation of cell cycle genes (TEDESCO *et al.* 2002; PILKINTON *et al.* 2007; BURKE *et al.* 2010). Thus, the association and dissociation of pocket proteins from their respective transcriptional

repressive complexes governs the switch between cell cycle quiescence and cell cycle progression.

The Rb-like homologs p130 and p107 represent the ancestral pocket proteins and likely the conserved components that mediate cell cycle control among eukaryotes (CAO *et al.* 2010; LIBAN *et al.* 2017). In *C. elegans*, LIN-35 is the sole pocket protein, most closely resembling p130/p107 (LU AND HORVITZ 1998). The pocket protein-associated complex MuvB was isolated in *Drosophila melanogaster* (KORENJAK *et al.* 2004; LEWIS *et al.* 2004) and *Caenorhabditis elegans* (HARRISON *et al.* 2006) before homologs were identified in mammals (LITOVCHICK *et al.* 2007; PILKINTON *et al.* 2007; SCHMIT *et al.* 2007). The *C. elegans* complex, called DRM, regulates cell cycle genes and requires MuvB to mediate gene repression (BOXEM AND VAN DEN HEUVEL 2002; GOETSCH *et al.* 2017). DRM also regulates cell fate specification by antagonizing Ras signaling during vulval development (MYERS AND GREENWALD 2005; CUI *et al.* 2006; HARRISON *et al.* 2006) and by protecting somatic cells from expressing germline genes (WANG *et al.* 2005; PETRELLA *et al.* 2011).

Extensive biochemical analyses have demonstrated how the DREAM complex forms on chromatin (Figure 1A) (LITOVCHICK *et al.* 2007; PILKINTON *et al.* 2007; SCHMIT *et al.* 2007; GUILEY *et al.* 2015). E2F-DP and LIN54, a MuvB component, direct site-specific chromatin localization (ZWICKER *et al.* 1995; SCHMIT *et al.* 2009; MULLER AND ENGELAND 2010; MULLER *et al.* 2012; MARCEAU *et al.* 2016). The Rb-like pocket protein serves as a bridge between the 2 DNA-binding DREAM components (GUILEY *et al.* 2015). The mammalian LIN52 protein interacts with the pocket protein via an “LxCxE motif” in LIN52. In mammals, the LxCxE motif is instead a suboptimal LxSxExL

sequence that is rendered optimal by phosphorylation of a nearby serine residue (S28) (GUILEY *et al.* 2015) (Figure 1B). S28 phosphorylation by DYRK1A kinase induces formation of mammalian DREAM (LITOVCHICK *et al.* 2011). In *C. elegans*, the conserved *lin-52* gene encodes the optimal LxCxE sequence (Figure 1B). *C. elegans* lacks a DYRK1A homolog and its corresponding consensus motif RxSP in LIN-52 (Figure 1B), suggesting that in *C. elegans* a phospho-switch likely does not induce DRM formation (LITOVCHICK *et al.* 2011; GUILEY *et al.* 2015). Importantly, the LxCxE binding motif mediates the high-affinity interaction that is employed by the human papillomavirus (HPV) viral oncoprotein E7 to disrupt association of LIN52 with mammalian pocket protein (GUILEY *et al.* 2015).

Here, we assessed how the Rb-like pocket protein contributes to DREAM complex formation and function on chromatin. We previously reported that the absence of LIN-35 results in a genome-wide decrease in chromatin occupancy of both E2F-DP and MuvB, illustrating how DRM/DREAM disassembly likely proceeds during cell cycle progression (GOETSCH *et al.* 2017). The model of DREAM complex assembly centers on reintroduction of the pocket protein associations with E2F-DP and MuvB as cells finish the cell cycle. To test this model, we used CRISPR/Cas9-mediated genome editing of the *C. elegans* LIN-52 subunit of MuvB to sever the association of the pocket protein with the MuvB subcomplex. Disrupting the *C. elegans* LIN-35-MuvB association caused a highly penetrant synthetic multivulval (SynMuv) phenotype, indicating that DRM antagonization of Ras signaling in the developing vulva, and thus its transcription repressive activity, was impaired. Chromatin immunoprecipitation revealed that the chromatin association of E2F-DP-LIN-35 and MuvB was not impaired by loss of LIN-35-

MuvB association. Finally, transcript analyses revealed that only 2 of 10 tested target genes became derepressed, suggesting that direct LIN-35-MuvB association potentiates, but is not required for, MuvB-mediated transcriptional repression. Together, this study highlights how the scaffolding activity of the pocket proteins facilitates transcriptional repression of target genes.

Materials and Methods

Worm strains

Strains were cultured on Nematode Growth Medium (NGM) agarose plates with *E. coli* OP50 and incubated at 20°C. The following strains were used:

Wild type N2 (Bristol)

SS1240: *lin-52(bn132(lin-52p::TagRFP-T^SEC^3xFLAG::lin-52 3' UTR)) III / hT2G [bli-4(e937) let-?(q782) qIs48] (I:III)*

SS1241: *lin-52(bn133(lin-52p::TagRFP-T::3xFLAG::lin-52 3' UTR)) III / hT2G [bli-4(e937) let-?(q782) qIs48] (I:III)*

SS1325: *lin-52(bn138(lin-52::GFP^SEC^3xFLAG)) III*

SS1256: *lin-52(bn139(lin-52::GFP::3xFLAG)) III*

SS1273: *lin-52(bn150(lin-52[C44A]::GFP::3xFLAG)) III*

SS1276: *lin-52(bn151(lin-52[L42A,C44A,E46A]::GFP ::3xFLAG)) III*

MT10591: *lin-8(n2731)*

MT1806: *lin-15A(n767)*

CRISPR/Cas9-mediated genome editing

For all genomic edits, 20 nucleotide crDNA targeting sequences were identified using the MIT CRISPR design tool (http://crispr.mit.edu). Single guide RNA sequences

were cloned into the PU6::unc119_sgRNA vector (Addgene plasmid #46169) using the overlapping PCR fragment method described in (FRIEDLAND *et al.* 2013) or were cloned into pDD162 (Addgene plasmid #47549) using the Q5 Site Directed Mutagenesis Kit (New England Biolabs), as described in (DICKINSON *et al.* 2013). Homologous repair templates were cloned into pDD282 (Addgene plasmid #66823) or pDD284 (Addgene plasmid #66825) using Glibson Assembly (New England Biolabs) (GIBSON *et al.* 2009), as described in (DICKINSON *et al.* 2015). CRISPR/Cas9 component plasmids were co-injected with marker plasmids (FROKJAER-JENSEN *et al.* 2008) to identify strains with an extra-chromosomal array instead of a mutated endogenous gene. For targeted mutagenesis, *dpy-10(cn64)* sgRNA (pJA58, Addgene plasmid #59933), and *dpy-10(cn64)* ssDNA template, *dpy-10(cn64)* guide and ssDNA template were co-injected to select for positive CRISPR activity in injectant progeny, as described in (ARRIBERE *et al.* 2014). Additional details are provided in Supplemental Materials and Methods.

Microscopy

L4 larvae were mounted on a 10% agarose pad and immobilized in a 1-2 µL suspension of 0.1 µm polystyrene beads (Polysciences), as described in (KIM *et al.* 2013). Fluorescence images were acquired using a Solamere spinning-disk confocal system with µManager software (EDELSTEIN *et al.* 2014). The microscope setup was as follows: Yokogawa CSUX-1 spinning disk scanner, Nikon TE2000-E inverted stand, Hamamatsu ImageEM X2 camera, solid state 405-, 488-, and 561-nm laser lines, 435–485, 500–550, and 573–613 fluorescent filters, and Nikon Plan Fluor 40x air objective. Images were processed using Image J (SCHNEIDER *et al.* 2012).

***C. elegans* phenotype scoring**

For brood size analyses, L4 individuals were cloned to fresh plates every 24 hours and all progeny were counted. For SynMuv phenotype scoring, 3 replicate plates per strain were set up with 5-10 adults that were allowed to lay eggs for 6 hours. Progeny were incubated at 20°C for 3 days, then scored for the presence or absence of pseudovulvae. The percentages of multivulva worms in each replicate population were averaged, and the standard deviation was calculated.

Immunoblotting and co-immunoprecipitation (coIP)

For immunoblotting whole worm lysates, 200 adults from each strain were picked into SDS gel-loading buffer (50 mM pH 6.8 Tris-Cl, 2% sodium dodecyl sulfate, 0.1% bromophenol blue, 100 mM β-mercaptoethanol). For coIP, embryos collected after bleaching gravid worms were aged for 3.5 hours and then frozen in liquid nitrogen, and lysates were prepared as described in (GOETSCH *et al.* 2017). For each IP, 8 mg of protein lysate was mixed with antibody-conjugated Dynabeads (ThermoFisher) and incubated for 2 hours at 4°C. Proteins were separated by SDS/PAGE, and western blot analysis was performed using a 1:1,000-1:5000 dilution of primary antibody and 1:2,000 dilution of an appropriate HRP-conjugated secondary antibody. Serial western blot analysis was performed by stripping the blot with buffer containing 0.2M pH 2.2 glycine, 0.1% SDS, and 1% Tween-20 between antibody probings. Additional details are provided in Supplemental Materials and Methods.

Chromatin immunoprecipitation (ChIP) and sequential ChIP

Embryos collected after bleaching gravid worms were aged for 3.5 hours and then frozen in liquid nitrogen. Lysates were prepared by grinding, crosslinking for 10 minutes in 1% formaldehyde, and sonicating to an average size of 250 base pairs in FA

207 buffer (50 mM HEPES/KOH pH 7.5, 1 mM EDTA, 1% Triton X-100, 0.1% sodium
208 deoxycholate, 150 mM NaCl) using a Bioruptor (Diagenode) on the high setting with 60
209 rounds of 30 seconds on and 1 minute rest. Protein concentrations of lysates were
210 determined using a Qubit fluorometer. ChIP and sequential ChIP experiments were
211 performed as described in (GOETSCH *et al.* 2017) and in Supplemental Materials and
212 Methods. Quantitative PCR was performed using SYBR green reagents on an Applied
213 Biosystems ViiA 7 Real-Time PCR System (ThermoFisher).

214 **Analysis of transcript levels by RT-qPCR**

215 Embryos collected after bleaching gravid worms were aged for 3.5 hours and
216 then frozen in Trizol for RNA isolation. A total of 1 µg RNA was treated with DNase and
217 reverse transcribed using the High Capacity cDNA Kit (Applied Biosystems). qPCR was
218 performed using SYBR green reagents on an Applied Biosystems ViiA 7 Real-Time
219 PCR System (ThermoFisher). The relative quantity of experimental transcripts was
220 calculated with *act-2* as the control gene using the ΔCt method.

221 **Quantification and statistical analysis**

222 For brood size analysis, significance was determined using a Wilcoxon-Mann-
223 Whitney test comparing CRISPR/Cas9-genome edited strains to wild type (N2). For
224 ChIP-qPCR and transcript level analysis by RT-qPCR, significance was determined
225 using a student's t-test between *lin-52(WT)* and *lin-52(1A)* and *lin-52(3A)* transgenic
226 strains.

227 **Data and reagent availability**

228 Requests for information, strains, and reagents should be directed to and will be
229 fulfilled by Paul D. Goetsch (pdgoetsc@mtu.edu). Primers used for cloning, ChIP-

qPCR, and RT-qPCR are available in Supplemental Table S1. All data necessary for confirming the conclusions present are represented fully within the article. Supplemental material is available at FigShare: XXX

Results

Targeted mutagenesis to disrupt DREAM complex formation

Structural studies previously demonstrated that MuvB interacts with the pocket protein via the LIN52 subunit (Figure 1A) (GUILEY *et al.* 2015). Using the self-excising cassette (SEC) method for *C. elegans* CRISPR/Cas9 genome editing (DICKINSON *et al.* 2015), we generated a *lin-52(KO)* strain (*lin52(bn133[lin-52p::TagRFP-T::3xFLAG]*) by completely replacing the *lin-52* gene with *TagRFP-T* coding sequence (Figure 2A). We observed that *lin-52(KO)* rendered worms sterile (Figure 2C), as previously observed in the *lin-52(n3718)* protein null strain (CEOL *et al.* 2006; HARRISON *et al.* 2006). This resembles loss of other MuvB components, as loss of LIN-9, LIN-53 (*C. elegans* RBAP48), or LIN-54 in protein null strains also renders worms sterile and affects the levels of other MuvB subunits, suggesting that MuvB components require co-expression for assembly/stability of the complex (HARRISON *et al.* 2006). Loss of LIN-37 does not cause sterility and does not affect assembly of the rest of MuvB in either *C. elegans* or mammalian cells (HARRISON *et al.* 2006; MAGES *et al.* 2017). We next replaced the *TagRFP-T* coding sequence with *lin-52* tagged with a C-terminal *GFP-3xFLAG* coding sequence, generating the *lin-52(WT)* strain (*lin-52(bn139[lin-52::GFP::3xFLAG]),* Figure 2A). We observed that *lin-52(WT)* completely rescued fertility (Figure 2C), indicating that the GFP tag does not disrupt LIN-52 function.

Since LIN-52 is essential for *C. elegans* fertility, we sought to disrupt the LIN-35-LIN-52 interaction without affecting protein integrity. We directed targeted mutagenesis of the LIN-52 LxCxE sequence (Figure 1B) using CRISPR/Cas9-mediated genomic editing. We generated 2 mutants of the LxCxE binding motif in *lin-52(WT)* using the *dpy-10* co-CRISPR method of small oligo homology-directed repair (ARRIBERE *et al.* 2014). We generated the *lin-52(1A)* single-alanine mutation strain (*lin-52(bn150[lin-52[C44A]::GFP::3xFLAG)*) and the *lin-52(3A)* triple-alanine mutation strain (*lin-52(bn151(lin-52[L42A,C44A,E46A]::GFP::3xFLAG)*) (Figure 2B) with the intent to completely disrupt LIN-52's interaction with the *C. elegans* pocket protein LIN-35. Additional silent mutations were included in the oligo repair templates to generate new restriction enzyme cut sites to aid in genotyping (Figure 2B).

Full loss of *C. elegans* DREAM activity causes sterility, as observed in protein null mutants of worm E2F-DP (*dpl-1* and *efl-1)* and worm MuvB (*lin-9, lin-52, lin-53, and lin-54)* (BEITEL *et al.* 2000; CHI AND REINKE 2006; TABUCHI *et al.* 2011). Since the C-terminally GFP-tagged *lin-52* coding sequence completely rescued *lin-52(KO)* sterility, we were able to test whether *lin-52(1A)* and *lin-52(3A)* disrupt DREAM function. We observed that neither the 1A nor 3A mutation in the LIN-52 LxCxE sequence caused a significant reduction in brood size (Figure 2C). Using western blot analysis of selected DREAM components from *lin-52(WT)* and mutant lysates, we observed that DREAM component protein levels were unaffected compared to wild type (N2) (Figure 2D, Figure S1). Similarly, using live image analysis of *lin-52(WT), lin-52(1A),* and *lin-52(3A)* L4 larvae, we observed that LIN-52 level and localization appeared normal in mutants (Figure 2A). Together, these results demonstrate that mutation of the LIN-52 LxCxE

sequence does not cause a *lin-52* null phenotype and does not alter the levels and tissue distribution of MuvB components.

Blocking DREAM complex formation causes the classic SynMuv mutant phenotype

C. elegans DREAM components were initially identified in genetic screens for a Synthetic Multivulval (SynMuv) phenotype (LU AND HORVITZ 1998; CEOL AND HORVITZ 2001; CEOL *et al.* 2006; HARRISON *et al.* 2006). All 8 components of DREAM were classified as SynMuv B genes; double mutant worms bearing a mutation in a SynMuv B gene along with a mutation in a SynMuv A gene have multiple vulvae along their ventral body instead of the usual single vulva (FAY AND YOCHEM 2007). We hypothesized that if DREAM function was affected by mutation of LIN-52's LxCxE sequence, then pairing our 1A and 3A LIN-52 mutations with a SynMuv A mutation should cause a SynMuv phenotype. When paired with SynMuv A allele *lin-8(n2731)* (HARRISON *et al.* 2007) or *lin-15A(n767)* (HUANG *et al.* 1994), *lin-52(3A)* but not with *lin-52(1A)* resulted in a SynMuv phenotype (Figure 3A). These results indicate that the 3A substitution in LxCxE impairs DREAM function.

To test whether the 3A substitution in fact impairs pocket protein-MuvB association, we performed co-immunoprecipitations (co-IPs) from protein extracts prepared from *lin-52(WT)*, *lin-52(1A)*, and *lin-52(3A)* late embryos. We pulled down LIN-35 and tested for LIN-52 association using the GFP epitope, and we pulled down LIN-52 using either the GFP or FLAG epitope and tested for LIN-35 association (Figure 3B, Figure S2). In both co-IP experiments, we observed that LIN-52 association with LIN-35 was lost in *lin-52(3A)* extracts but not in *lin-52(1A)* extracts. These results demonstrate

298 that the LIN-52 3A substitution successfully severed the protein-protein association
299 between LIN-52 and LIN-35, effectively blocking formation of an intact DREAM
300 complex.

301 **E2F-DP-LIN-35 and MuvB subcomplexes independently co-occupy chromatin**
302 **sites**

303 In the absence of LIN-35, E2F-DP and MuvB do not associate with one another
304 and their chromatin occupancy is reduced genome-wide (GOETSCH *et al.* 2017). In our
305 *lin-52(3A)* worm strain, LIN-35 is present, but its association with MuvB is severed. We
306 tested the impact of this severing on the chromatin localization of DREAM components
307 using chromatin immunoprecipitation (ChIP). We chose 4 genes, *set-21, mis-12, polh-1,*
308 and *air-1,* as representative DREAM target genes; in *lin-35* null embryos, the chromatin
309 occupancy of DREAM components was greatly diminished at each of their gene
310 promoters and was undetectable at the *air-1* promoter (GOETSCH *et al.* 2017). We
311 observed that all tested DREAM components remained similarly enriched at the 4
312 selected promoters in *lin-52(3A)* as compared to *lin-52(WT)* (Figure 4A). An additional 6
313 DREAM target gene promoters were tested and showed similar DREAM occupancy
314 profiles (Figure S3A). The DREAM components tested included E2F-DP (DPL-1 and
315 EFL-1) and LIN-35, suggesting that the chromatin association of the repressive E2F-DP
316 transcription factor heterodimer is stabilized by its interaction with the pocket protein.

317 To test whether MuvB and E2F-DP-LIN-35 co-occupy DREAM target regions, we
318 performed sequential ChIP analysis. We first ChIPed LIN-52 via its FLAG tag and then
319 ChIPed LIN-35. We observed no significant difference in LIN-35 co-occupancy in *lin-*
320 *52(3A)* extracts versus *lin-52(WT)* extracts (Figure 4B). Our results indicate that,

although the interaction of LIN-35 and MuvB is disrupted, DREAM components nevertheless co-localize at target promoters through their respective protein-DNA interactions.

Severing the LIN-35-MuvB connection impairs transcriptional repression of some but not all DREAM target genes

MuvB dissociation from E2F-DP-LIN-35 resulted in no observed decline in chromatin occupancy of DREAM at the 10 gene promoters tested (Figure 4A, Figure S3A). Each of the gene products targeted by the 4 selected promoter regions in Figure 4A was upregulated in the *lin-35* null strain (KIRIENKO AND FAY 2007; GOETSCH *et al.* 2017). We performed gene expression analysis of these 4 genes in *lin-52(WT)*, *lin-52(1A)*, and *lin-52(3A)* late embryos using RT-qPCR (Figure 4C). We observed that 2 genes, *set-21* and *polh-1*, were significantly upregulated in both *lin-52* mutant strains, while 2 genes, *mis-12* and *air-1*, were not up-regulated. Transcript levels of the gene products targeted by the 6 selected promoter regions in Figure S3A were not affected (Figure S3B). Importantly, in the *lin-35* null strain, DREAM was dissociated from the *air-1* promoter and *air-1* was upregulated (GOETSCH *et al.* 2017). In our study, DREAM (with a severed LIN-35-LIN-52 connection) was associated with the *air-1* promoter and *air-1* was not upregulated. Thus, MuvB chromatin occupancy is necessary but not sufficient for repression of DREAM target genes.

Discussion

The trio of pocket proteins, pRb, p107, and p130, govern cell cycle exit and reentry through targeted transcriptional repression of cell cycle genes. We analyzed how the sole *C. elegans* Rb-like pocket protein LIN-35 contributes to the formation and

function of the DREAM complex, which relies on the recruitment of the highly conserved and essential 5-subunit MuvB complex to direct repression of target genes. Using CRISPR/Cas9-mediated targeted mutagenesis, we generated a mutant *C. elegans* strain in which MuvB's LIN-35-interacting subunit LIN-52 was rendered incapable of interacting with LIN-35. Blocking DREAM assembly in worms impaired DREAM function, causing the classic SynMuv phenotype and upregulation of some DREAM target genes. However, even though LIN-35 and MuvB association was abolished, all of the DREAM components tested showed unimpaired association with chromatin. Thus, our findings reveal that the LIN-35-MuvB association potentiates MuvB-mediated transcriptional repression but is not required.

Our analysis provides important insight into how assembly of the mammalian DREAM complex establishes repression of cell cycle genes. DREAM assembly is triggered by DYRK1A phosphorylation of LIN52, initiating MuvB association with p107/p130 (LITOVCHICK *et al.* 2011; GUILEY *et al.* 2015). Mammalian MuvB's function switches between transcriptional repression in the DREAM complex during quiescence and transcriptional activation after associating with the B-Myb transcription factor and forming the Myb-MuvB (MMB) complex during the late cell cycle (LEWIS *et al.* 2004; OSTERLOH *et al.* 2007; SCHMIT *et al.* 2007; KNIGHT *et al.* 2009; SADASIVAM *et al.* 2012). DYRK1A-mediated LIN52 phosphorylation also inhibits MuvB association with B-Myb (LITOVCHICK *et al.* 2011), even though the 2 interaction interfaces are not exclusive (GUILEY *et al.* 2018). Our data demonstrate that MuvB localizes to chromatin sites and represses gene targets without direct association with the pocket protein. Thus, we

366 propose that the pocket protein's primary role in DREAM complex assembly is to protect
367 MuvB's function as a transcriptional repressor.

368 The delicate switch between MuvB-associated cell cycle gene repression and
369 activation is hijacked in cancer cells. All 3 mammalian pocket proteins are inactivated by
370 the E7 viral oncoprotein present in high-risk human papillovirus (HPV) (ZHANG *et al.*
371 2006; HUH *et al.* 2007). E7 interacts with the mammalian pocket proteins through the
372 high-affinity LxCxE binding motif, disrupting MuvB association in DREAM (GUILEY *et al.*
373 2015). HPV E7 concurrently coaxes MuvB into its transcriptional activator function by
374 stimulating MMB assembly (PANG *et al.* 2014). However, cancer cells resist cytotoxic
375 chemotherapy by temporarily exiting the cell cycle (BOICHUK *et al.* 2013), suggesting
376 that MuvB's capacity for transcriptional repression is retained. Based on our findings
377 that MuvB does not require direct association with the pocket protein to target gene
378 repression, we propose that MuvB's function in cancer cells requires closer scrutiny.

379 We previously observed that E2F-DP and MuvB chromatin association is
380 severely affected by loss of LIN-35 (GOETSCH *et al.* 2017). By severing LIN-35-MuvB
381 association, this study reveals that LIN-35 directly stabilizes E2F-DP chromatin
382 occupancy. However, we also observed that MuvB chromatin occupancy is not impaired
383 even though MuvB no longer associates directly with E2F-DP-LIN-35. Importantly, *in*
384 *vitro* analysis of heterodimeric mammalian E2F-DP complex DNA binding
385 characteristics identified a distinct induction of DNA bending, especially in the case of
386 the homologues of *C. elegans* EFL-1-DPL-1 (E2F4-DP1/2) (TAO *et al.* 1997). We
387 propose that DREAM-associated E2F-DP heterodimers promote MuvB co-occupancy
388 through a DNA bending-dependent mechanism. Together, our results suggest a model

in which the LIN-35 pocket protein promotes E2F-DP chromatin occupancy, which in turn promotes MuvB chromatin occupancy.

Our results support an exciting model for how local E2F-DP-mediated alterations to DNA shape enhanced by their interaction with a pocket protein promote MuvB co-occupancy. Even with evolutionary divergence from the ancestral pocket protein, this model may also apply to pRb function. Many histone deacetylases and chromatin remodeling complexes associate with pRb through the LxCxE binding cleft, although many of these associations have only limited support thus far from structural/biochemical interaction studies (DYSON 2016). Variation in pRb monophosphorylation events that can alter pRb structure and recognition of binding partners offer one explanation for how pRb can potentially interact with >300 individual protein partners (RUBIN 2013; NARASIMHA *et al.* 2014). Our data provide an alternative, but not exclusive, possibility, namely that direct and stable pRb association with these myriad protein partners may be unnecessary. Perhaps pRb association with a few partners such as E2F-DPs promotes localization of multi-protein complexes to genomic sites. Additional dissection of DREAM and pRb structure and function will shed light on how the pocket proteins mediate their essential cellular roles.

Acknowledgments

We thank Seth Rubin and members of the Rubin and Strome labs for helpful discussions. Some strains were provided by the Caenorhabditis Genetics Center, which is funded by the NIH Office of Research Infrastructure Programs (P40 OD010440). This work was supported by National Institutes of Health R01 grant GM34069 to S.S. and American Cancer Society Postdoctoral Fellowship PF-16-106-01-DDC to P.D.G.

Figure 1

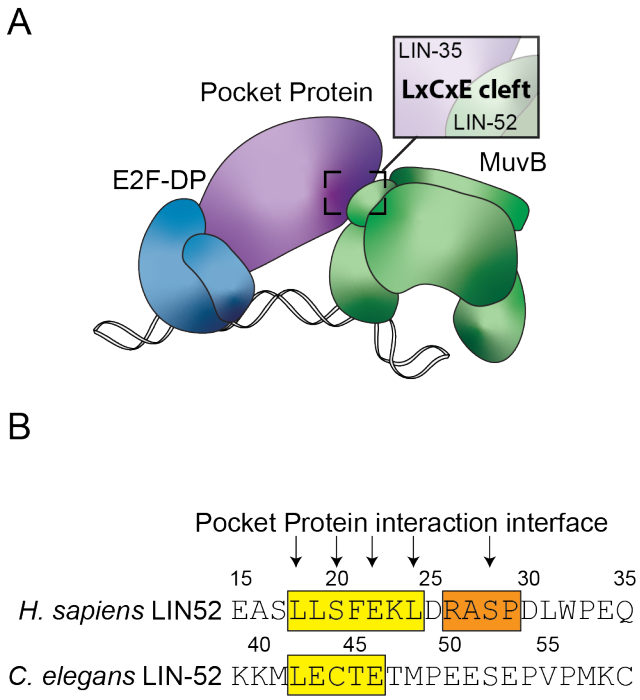

Figure 1 Model of DREAM complex formation

(A) Model of the *C. elegans* DREAM complex bound to DNA: E2F-DP (blue), the pocket protein LIN-35 (purple), and the 5-subunit MuvB subcomplex (green). The highlighted region shows the target region for this study: an LxCxE binding motif in the MuvB subunit LIN-52 that interacts directly with the LIN-35 pocket protein.

(B) Alignment of *H. sapiens* LIN52 and *C. elegans* LIN-52 sequences. The human LxSxExL and worm LxCxE sequences are highlighted in yellow, and the human DYRK1A consensus phosphorylation sequence is highlighted in orange. Arrows indicate residues involved in the interaction with the pocket protein.

Figure 2

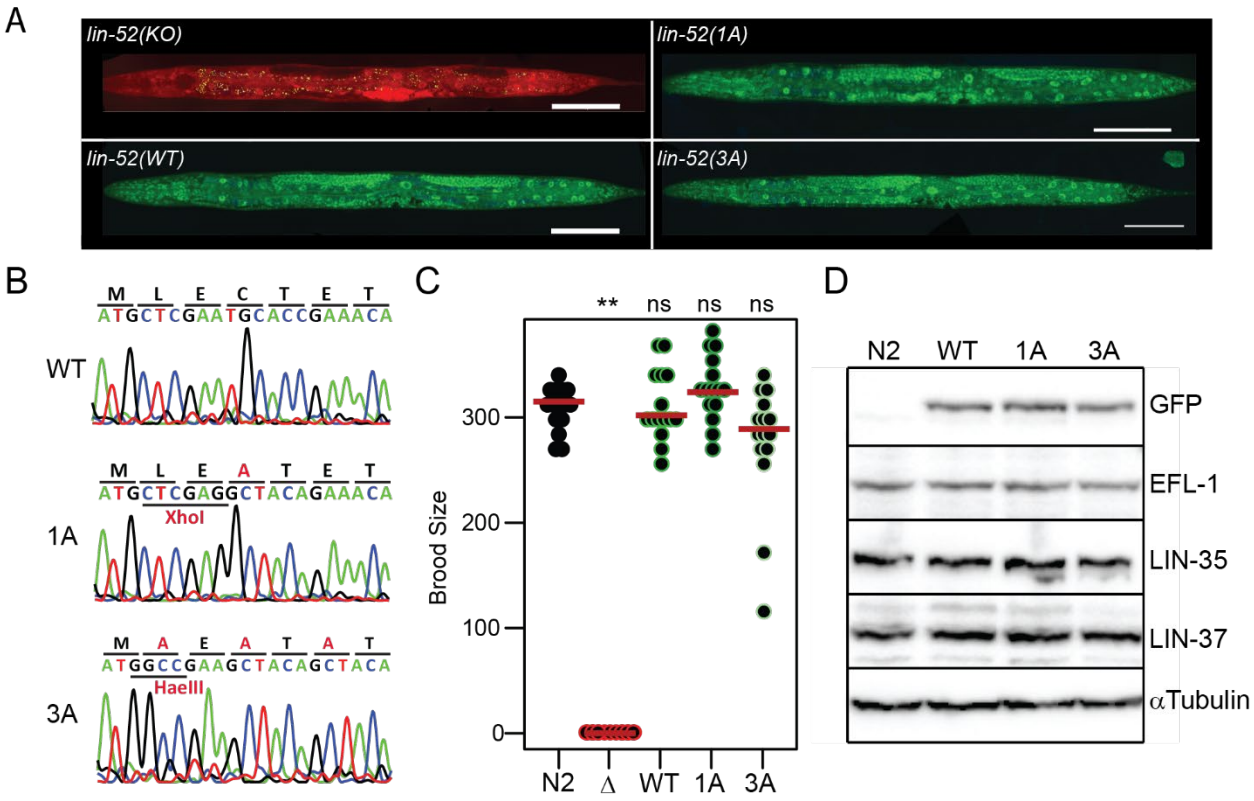

Figure 2 Targeted mutagenesis to disrupt DREAM complex formation

(A) Live worm fluorescence images of *lin-52(KO), lin-52(WT*), *lin-52(1A),* and *lin-52(3A)* L4 larvae. Composites were artificially straightened. Scale bar, 100μM.

(B) Sanger sequencing of the *lin-52* LxCxE coding region in *lin-52(WT), lin-52(1A*), and *lin-52(3A*).

(C) Strip chart of the brood sizes of wild-type (N2) worms and *lin-52(KO)*, *lin-52(WT)*, *lin-52(1A)*, and *lin-52(3A)* transgenic worms. Significance (** p-value < 0.01) was determined by a Wilcoxon-Mann-Whitney test comparing the indicated strains to wild type (N2).

(D) Western blot analysis of DREAM subunits LIN-52 (via GFP tag), EFL-1, LIN-35, and LIN-37 using lysates from wild-type (N2) worms and *lin-52(WT), lin-52(1A),* and *lin-*

458 *52(3A)* transgenic worms separated by SDS/PAGE. Antibodies used are indicated on
459 the right. Alpha-tubulin was used as a loading control. Full blots are shown in Figure S1.
460
461
462
463
464
465
466
467
468
469
470
471
472
473
474
475
476
477
478
479
480

Figure 3

A

% SynMuv±s.d. (n)	*lin-8(n2731)*	*lin-15A(n767)*
WT	0±0 (382)	0±0 (505)
1A	0±0 (211)	0±0 (422)
3A	99.3±0.6 (301)	96.5±0.2 (375)

B

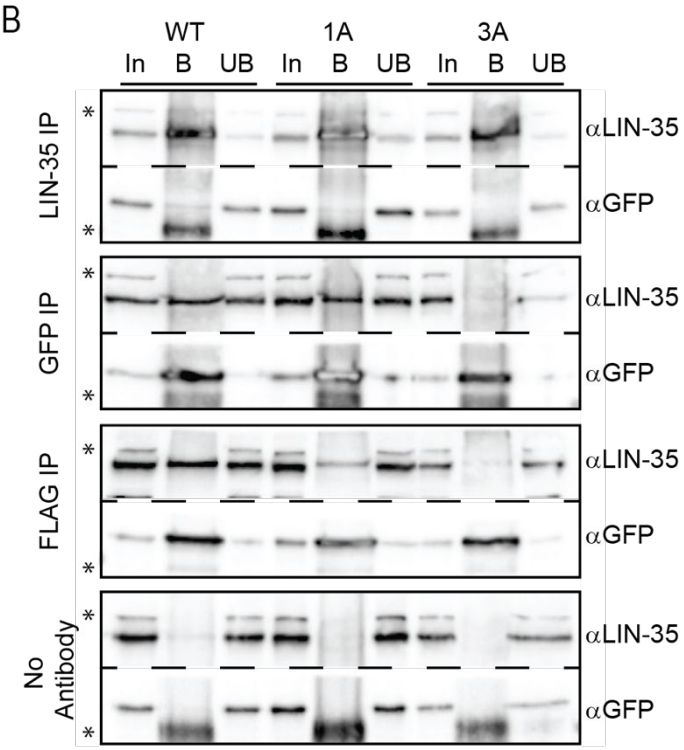

Figure 3 Blocking DREAM complex formation recapitulates the classic SynMuv phenotype

(A) Table indicating the percentage Synthetic Multivulval (SynMuv) of *lin-52(WT), lin-52(1A)*, and *lin-52(3A)* in combination with SynMuv A mutant alleles *lin-8(n2731)* or *lin-15A(n767)* with standard deviation indicated. The population size (n*)* is indicated in parentheses.

(B) Late embryo extracts from *lin-52(WT)*, *lin-52(1A)*, and *lin-52(3A)* (each tagged with GFP and FLAG) were immunoprecipitated with anti-LIN-35, anti-GFP, and anti-FLAG antibodies, with no antibody serving as a negative control. Proteins bound (B) and unbound (UB) were separated by SDS/PAGE, and western blot analysis was performed using the antibodies indicated on the right. 5% of Input (In) is shown on the left. Asterisks indicate non-specific bands. Full blots are shown in Figure S2.

526 **Figure 4**

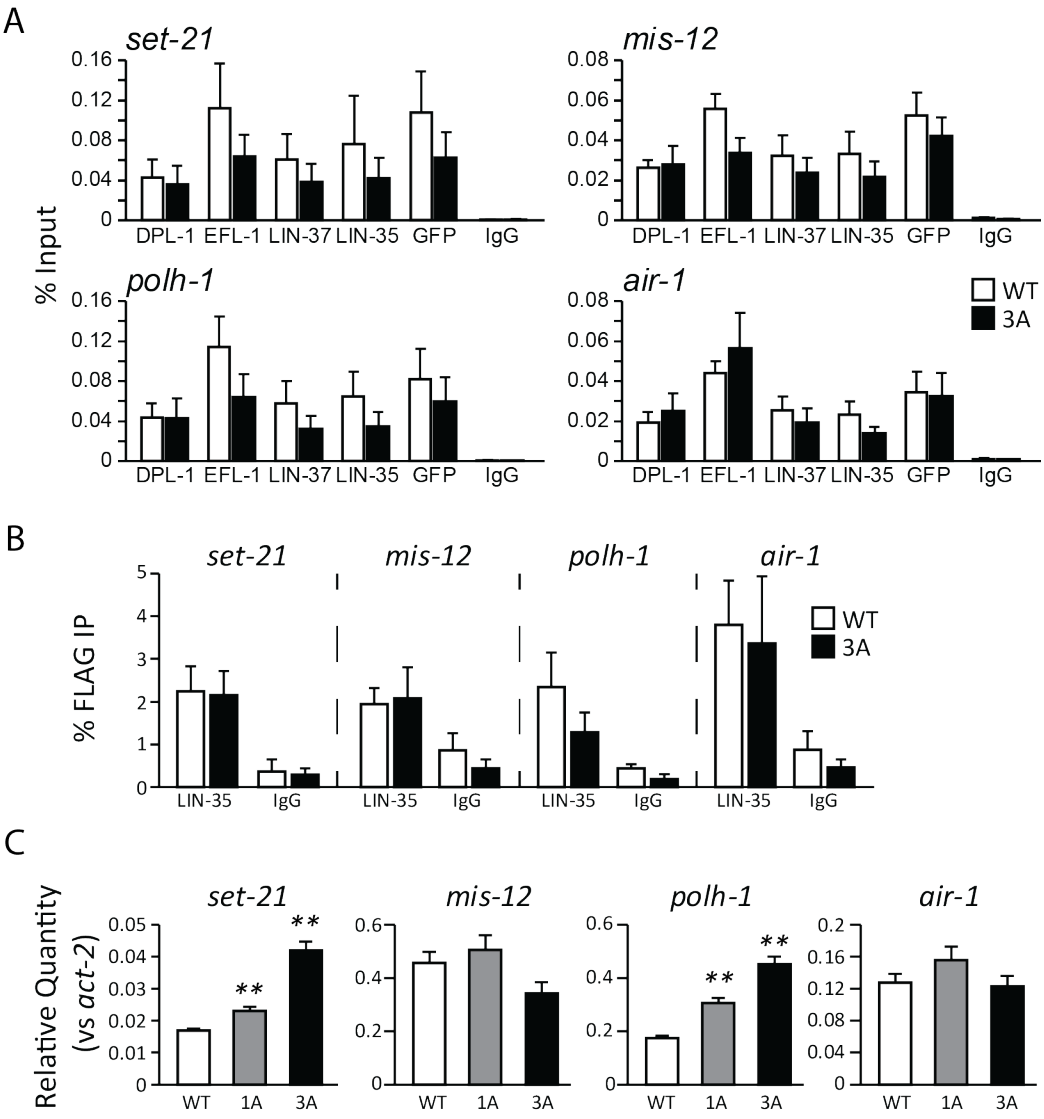

527

528 **Figure 4 Analysis of chromatin association with and repression of DREAM target**

529 **genes**

530 (A) ChIP-qPCR of 5 DREAM subunits DPL-1, EFL-1, LIN-37, LIN-35, and LIN-52 (via

531 GFP tag) from *lin-52(WT*) (white) and *lin-52(3A*) (black) late embryo extracts at 4

532 DREAM target genes. IgG was used as a negative control. Signals are presented as

533 percentage of Input DNA. Error bars indicate standard error of the mean. Additional

534 target genes are shown in Figure S3.

(B) Sequential ChIP-qPCR of LIN-52 (via FLAG tag) followed by LIN-35 or IgG from *lin-52(WT*) (white) and *lin-52(3A*) (black) late embryo extracts at 4 DREAM target genes. Signals are presented as percentage of FLAG IP DNA. Error bars indicate standard error of the mean.

(C) RT-qPCR analysis comparing transcript levels of 4 DREAM target genes in *lin-52(WT)* (white) *lin-52(1A)* (grey), and *lin-52(3A)* (black) late embryos. Expression values from 2 independent experiments each consisting of 4 biological replicates were averaged and are presented as the relative quantity (Rq) compared to *act-2.* Error bars indicate standard error of the mean, and significance was determined by a student's T-test between transcript levels in mutant (3A or 1A) vs WT (** p-value < 0.01). Additional target genes are shown in Figure S3.

References

Arribere, J. A., R. T. Bell, B. X. Fu, K. L. Artiles, P. S. Hartman *et al.*, 2014 Efficient marker-free recovery of custom genetic modifications with CRISPR/Cas9 in Caenorhabditis elegans. Genetics 198**:** 837-846.

Beitel, G. J., E. J. Lambie and H. R. Horvitz, 2000 The C. elegans gene lin-9,which acts in an Rb-related pathway, is required for gonadal sheath cell development and encodes a novel protein. Gene 254**:** 253-263.

Boichuk, S., J. A. Parry, K. R. Makielski, L. Litovchick, J. L. Baron *et al.*, 2013 The DREAM complex mediates GIST cell quiescence and is a novel therapeutic target to enhance imatinib-induced apoptosis. Cancer Res 73**:** 5120-5129.

Boxem, M., and S. van den Heuvel, 2002 C. elegans class B synthetic multivulva genes act in G(1) regulation. Curr Biol 12**:** 906-911.

Burke, J. R., A. J. Deshong, J. G. Pelton and S. M. Rubin, 2010 Phosphorylation-induced conformational changes in the retinoblastoma protein inhibit E2F transactivation domain binding. J Biol Chem 285**:** 16286-16293.

Burkhart, D. L., and J. Sage, 2008 Cellular mechanisms of tumour suppression by the retinoblastoma gene. Nat Rev Cancer 8**:** 671-682.

Cao, L., B. Peng, L. Yao, X. Zhang, K. Sun *et al.*, 2010 The ancient function of RB-E2F pathway: insights from its evolutionary history. Biol Direct 5**:** 55.

Ceol, C. J., and H. R. Horvitz, 2001 dpl-1 DP and efl-1 E2F act with lin-35 Rb to antagonize Ras signaling in C. elegans vulval development. Mol Cell 7**:** 461-473.

579 Ceol, C. J., F. Stegmeier, M. M. Harrison and H. R. Horvitz, 2006 Identification and
580 classification of genes that act antagonistically to let-60 Ras signaling in
581 Caenorhabditis elegans vulval development. Genetics 173**:** 709-726.
582 Chi, W., and V. Reinke, 2006 Promotion of oogenesis and embryogenesis in the C.
583 elegans gonad by EFL-1/DPL-1 (E2F) does not require LIN-35 (pRB).
584 Development 133**:** 3147-3157.
585 Classon, M., and N. Dyson, 2001 p107 and p130: versatile proteins with interesting
586 pockets. Exp Cell Res 264**:** 135-147.
587 Classon, M., and E. Harlow, 2002 The retinoblastoma tumour suppressor in development
588 and cancer. Nat Rev Cancer 2**:** 910-917.
589 Cobrinik, D., 2005 Pocket proteins and cell cycle control. Oncogene 24**:** 2796-2809.
590 Cui, M., J. Chen, T. R. Myers, B. J. Hwang, P. W. Sternberg *et al.*, 2006 SynMuv genes
591 redundantly inhibit lin-3/EGF expression to prevent inappropriate vulval induction
592 in C. elegans. Dev Cell 10**:** 667-672.
593 Dick, F. A., and S. M. Rubin, 2013 Molecular mechanisms underlying RB protein function.
594 Nat Rev Mol Cell Biol 14**:** 297-306.
595 Dickinson, D. J., A. M. Pani, J. K. Heppert, C. D. Higgins and B. Goldstein, 2015
596 Streamlined Genome Engineering with a Self-Excising Drug Selection Cassette.
597 Genetics 200**:** 1035-1049.
598 Dickinson, D. J., J. D. Ward, D. J. Reiner and B. Goldstein, 2013 Engineering the
599 Caenorhabditis elegans genome using Cas9-triggered homologous
600 recombination. Nat Methods 10**:** 1028-1034.

Dyson, N. J., 2016 RB1: a prototype tumor suppressor and an enigma. Genes Dev 30: 1492-1502.

Edelstein, A. D., M. A. Tsuchida, N. Amodaj, H. Pinkard, R. D. Vale *et al.*, 2014 Advanced methods of microscope control using muManager software. J Biol Methods 1.

Fay, D. S., and J. Yochem, 2007 The SynMuv genes of Caenorhabditis elegans in vulval development and beyond. Dev Biol 306: 1-9.

Friedland, A. E., Y. B. Tzur, K. M. Esvelt, M. P. Colaiacovo, G. M. Church *et al.*, 2013 Heritable genome editing in C. elegans via a CRISPR-Cas9 system. Nat Methods 10: 741-743.

Frokjaer-Jensen, C., M. W. Davis, C. E. Hopkins, B. J. Newman, J. M. Thummel *et al.*, 2008 Single-copy insertion of transgenes in Caenorhabditis elegans. Nat Genet 40: 1375-1383.

Gibson, D. G., L. Young, R. Y. Chuang, J. C. Venter, C. A. Hutchison, 3rd *et al.*, 2009 Enzymatic assembly of DNA molecules up to several hundred kilobases. Nat Methods 6: 343-345.

Goetsch, P. D., J. M. Garrigues and S. Strome, 2017 Loss of the Caenorhabditis elegans pocket protein LIN-35 reveals MuvB's innate function as the repressor of DREAM target genes. PLoS Genet 13: e1007088.

Guiley, K. Z., A. N. Iness, S. Saini, S. Tripathi, J. S. Lipsick *et al.*, 2018 Structural mechanism of Myb-MuvB assembly. Proc Natl Acad Sci U S A 115: 10016-10021.

Guiley, K. Z., T. J. Liban, J. G. Felthousen, P. Ramanan, L. Litovchick *et al.*, 2015 Structural mechanisms of DREAM complex assembly and regulation. Genes Dev 29: 961-974.

624 Harrison, M. M., C. J. Ceol, X. Lu and H. R. Horvitz, 2006 Some C. elegans class B
625 synthetic multivulva proteins encode a conserved LIN-35 Rb-containing complex
626 distinct from a NuRD-like complex. Proc Natl Acad Sci U S A 103**:** 16782-16787.
627 Harrison, M. M., X. Lu and H. R. Horvitz, 2007 LIN-61, one of two Caenorhabditis elegans
628 malignant-brain-tumor-repeat-containing proteins, acts with the DRM and NuRD-
629 like protein complexes in vulval development but not in certain other biological
630 processes. Genetics 176**:** 255-271.
631 Helin, K., J. A. Lees, M. Vidal, N. Dyson, E. Harlow *et al.*, 1992 A cDNA encoding a pRB-
632 binding protein with properties of the transcription factor E2F. Cell 70**:** 337-350.
633 Huang, L. S., P. Tzou and P. W. Sternberg, 1994 The lin-15 locus encodes two negative
634 regulators of Caenorhabditis elegans vulval development. Mol Biol Cell 5**:** 395-
635 411.
636 Huh, K., X. Zhou, H. Hayakawa, J. Y. Cho, T. A. Libermann *et al.*, 2007 Human
637 papillomavirus type 16 E7 oncoprotein associates with the cullin 2 ubiquitin ligase
638 complex, which contributes to degradation of the retinoblastoma tumor
639 suppressor. J Virol 81**:** 9737-9747.
640 Hurford, R. K., Jr., D. Cobrinik, M. H. Lee and N. Dyson, 1997 pRB and p107/p130 are
641 required for the regulated expression of different sets of E2F responsive genes.
642 Genes Dev 11**:** 1447-1463.
643 Kim, E., L. Sun, C. V. Gabel and C. Fang-Yen, 2013 Long-term imaging of Caenorhabditis
644 elegans using nanoparticle-mediated immobilization. PLoS One 8**:** e53419.
645 Kirienko, N. V., and D. S. Fay, 2007 Transcriptome profiling of the C. elegans Rb ortholog
646 reveals diverse developmental roles. Dev Biol 305**:** 674-684.

647 Knight, A. S., M. Notaridou and R. J. Watson, 2009 A Lin-9 complex is recruited by B-
648 Myb to activate transcription of G2/M genes in undifferentiated embryonal
649 carcinoma cells. Oncogene 28**:** 1737-1747.
650 Korenjak, M., B. Taylor-Harding, U. K. Binne, J. S. Satterlee, O. Stevaux *et al.*, 2004
651 Native E2F/RBF complexes contain Myb-interacting proteins and repress
652 transcription of developmentally controlled E2F target genes. Cell 119**:** 181-193.
653 Lees, J. A., M. Saito, M. Vidal, M. Valentine, T. Look *et al.*, 1993 The retinoblastoma
654 protein binds to a family of E2F transcription factors. Mol Cell Biol 13**:** 7813-7825.
655 Lewis, P. W., E. L. Beall, T. C. Fleischer, D. Georlette, A. J. Link *et al.*, 2004 Identification
656 of a Drosophila Myb-E2F2/RBF transcriptional repressor complex. Genes Dev 18**:**
657 2929-2940.
658 Liban, T. J., E. M. Medina, S. Tripathi, S. Sengupta, R. W. Henry *et al.*, 2017 Conservation
659 and divergence of C-terminal domain structure in the retinoblastoma protein family.
660 Proc Natl Acad Sci U S A 114**:** 4942-4947.
661 Liban, T. J., M. J. Thwaites, F. A. Dick and S. M. Rubin, 2016 Structural Conservation
662 and E2F Binding Specificity within the Retinoblastoma Pocket Protein Family. J
663 Mol Biol 428**:** 3960-3971.
664 Litovchick, L., L. A. Florens, S. K. Swanson, M. P. Washburn and J. A. DeCaprio, 2011
665 DYRK1A protein kinase promotes quiescence and senescence through DREAM
666 complex assembly. Genes Dev 25**:** 801-813.
667 Litovchick, L., S. Sadasivam, L. Florens, X. Zhu, S. K. Swanson *et al.*, 2007 Evolutionarily
668 conserved multisubunit RBL2/p130 and E2F4 protein complex represses human
669 cell cycle-dependent genes in quiescence. Mol Cell 26**:** 539-551.

Lu, X., and H. R. Horvitz, 1998 lin-35 and lin-53, two genes that antagonize a C. elegans Ras pathway, encode proteins similar to Rb and its binding protein RbAp48. Cell 95**:** 981-991.

Mages, C. F., A. Wintsche, S. H. Bernhart and G. A. Muller, 2017 The DREAM complex through its subunit Lin37 cooperates with Rb to initiate quiescence. Elife 6.

Marceau, A. H., J. G. Felthousen, P. D. Goetsch, A. N. Iness, H. W. Lee *et al.*, 2016 Structural basis for LIN54 recognition of CHR elements in cell cycle-regulated promoters. Nat Commun 7**:** 12301.

Muller, G. A., and K. Engeland, 2010 The central role of CDE/CHR promoter elements in the regulation of cell cycle-dependent gene transcription. FEBS J 277**:** 877-893.

Muller, G. A., M. Quaas, M. Schumann, E. Krause, M. Padi *et al.*, 2012 The CHR promoter element controls cell cycle-dependent gene transcription and binds the DREAM and MMB complexes. Nucleic Acids Res 40**:** 1561-1578.

Muller, G. A., K. Stangner, T. Schmitt, A. Wintsche and K. Engeland, 2017 Timing of transcription during the cell cycle: Protein complexes binding to E2F, E2F/CLE, CDE/CHR, or CHR promoter elements define early and late cell cycle gene expression. Oncotarget 8**:** 97736-97748.

Myers, T. R., and I. Greenwald, 2005 lin-35 Rb acts in the major hypodermis to oppose ras-mediated vulval induction in C. elegans. Dev Cell 8**:** 117-123.

Narasimha, A. M., M. Kaulich, G. S. Shapiro, Y. J. Choi, P. Sicinski *et al.*, 2014 Cyclin D activates the Rb tumor suppressor by mono-phosphorylation. Elife 3.

691 Osterloh, L., B. von Eyss, F. Schmit, L. Rein, D. Hubner *et al.*, 2007 The human synMuv-
692 like protein LIN-9 is required for transcription of G2/M genes and for entry into
693 mitosis. EMBO J 26**:** 144-157.
694 Pang, C. L., S. Y. Toh, P. He, S. Teissier, Y. Ben Khalifa *et al.*, 2014 A functional
695 interaction of E7 with B-Myb-MuvB complex promotes acute cooperative
696 transcriptional activation of both S- and M-phase genes. (129 c). Oncogene 33**:**
697 4039-4049.
698 Petrella, L. N., W. Wang, C. A. Spike, A. Rechtsteiner, V. Reinke *et al.*, 2011 synMuv B
699 proteins antagonize germline fate in the intestine and ensure C. elegans survival.
700 Development 138**:** 1069-1079.
701 Pilkinton, M., R. Sandoval and O. R. Colamonici, 2007 Mammalian Mip/LIN-9 interacts
702 with either the p107, p130/E2F4 repressor complex or B-Myb in a cell cycle-phase-
703 dependent context distinct from the Drosophila dREAM complex. Oncogene 26**:**
704 7535-7543.
705 Rubin, S. M., 2013 Deciphering the retinoblastoma protein phosphorylation code. Trends
706 Biochem Sci 38**:** 12-19.
707 Sadasivam, S., S. Duan and J. A. DeCaprio, 2012 The MuvB complex sequentially
708 recruits B-Myb and FoxM1 to promote mitotic gene expression. Genes Dev 26**:**
709 474-489.
710 Schmit, F., S. Cremer and S. Gaubatz, 2009 LIN54 is an essential core subunit of the
711 DREAM/LINC complex that binds to the cdc2 promoter in a sequence-specific
712 manner. FEBS J 276**:** 5703-5716.

713 Schmit, F., M. Korenjak, M. Mannefeld, K. Schmitt, C. Franke *et al.*, 2007 LINC, a human
714 complex that is related to pRB-containing complexes in invertebrates regulates the
715 expression of G2/M genes. Cell Cycle 6**:** 1903-1913.
716 Schneider, C. A., W. S. Rasband and K. W. Eliceiri, 2012 NIH Image to ImageJ: 25 years
717 of image analysis. Nat Methods 9**:** 671-675.
718 Tabuchi, T. M., B. Deplancke, N. Osato, L. J. Zhu, M. I. Barrasa *et al.*, 2011 Chromosome-
719 biased binding and gene regulation by the Caenorhabditis elegans DRM complex.
720 PLoS Genet 7**:** e1002074.
721 Tao, Y., R. F. Kassatly, W. D. Cress and J. M. Horowitz, 1997 Subunit composition
722 determines E2F DNA-binding site specificity. Mol Cell Biol 17**:** 6994-7007.
723 Tedesco, D., J. Lukas and S. I. Reed, 2002 The pRb-related protein p130 is regulated by
724 phosphorylation-dependent proteolysis via the protein-ubiquitin ligase SCF(Skp2).
725 Genes Dev 16**:** 2946-2957.
726 Wang, D., S. Kennedy, D. Conte, Jr., J. K. Kim, H. W. Gabel *et al.*, 2005 Somatic
727 misexpression of germline P granules and enhanced RNA interference in
728 retinoblastoma pathway mutants. Nature 436**:** 593-597.
729 Zhang, B., W. Chen and A. Roman, 2006 The E7 proteins of low- and high-risk human
730 papillomaviruses share the ability to target the pRB family member p130 for
731 degradation. Proc Natl Acad Sci U S A 103**:** 437-442.
732 Zwicker, J., F. C. Lucibello, L. A. Wolfraim, C. Gross, M. Truss *et al.*, 1995 Cell cycle
733 regulation of the cyclin A, cdc25C and cdc2 genes is based on a common
734 mechanism of transcriptional repression. EMBO J 14**:** 4514-4522.

735

Supplemental Information

DREAM Interrupted: Severing MuvB from DREAM's pocket protein in *Caenorhabditis elegans* impairs gene repression but not DREAM chromatin assembly

Paul D. Goetsch and Susan Strome

Supplemental Materials and Methods:

CRISPR/Cas9-mediated genome editing

To generate *lin-52(KO),* 2 Cas9 target sites were identified near the 5' and 3' ends of the *lin-52 gene*. Single guide RNA sequences were cloned into the PU6::unc119_sgRNA vector. The *lin-52* KO homologous repair template was generated by amplifying homology arms containing the *lin-52* promoter and *lin-52* 3' UTR and cloned into the N-terminal tag digested pDD284 vector. The following injection mix was microinjected into the germline of ~50 N2 young adults: 50 ng / µL Cas9 expression plasmid (pDD162, Addgene #47549), 2.5 ng / µL *Pmyo-2::mCherry::unc-54utr* (pCJF90, Addgene #19327), 5 ng / µL *Pmyo-3::mCherry::unc-54utr* (pCFJ104, Addgene #19328), 10 ng / µL *Prab-3::mCherry::unc-54utr* (pGH8, Addgene #19359), 50 ng / µL *lin-52* 5' sgRNA (pPDG14), 50 ng / µL *lin-52* 3' sgRNA (pPDG18), and 10 ng µL *Plin-52::TagRFP-T^SEC^3xFLAG::lin-52utr* (pPDG13). CRISPR/Cas9-positive progeny were treated with hygromycin and screened for the Roller phenotype and absence of fluorescent co-injection marker expression (the latter enables extrachromosomal arrays to be distinguished from edited endogenous genes). Individuals from 1 positive selection plate were selected and balanced to create the strain SS1240 *lin-52(bn132(lin-52p::TagRFP-T^SEC^3xFLAG::lin-52 3' UTR)) III / hT2G [bli-4(e937) let-?(q782) qIs48] (I;III)*. The self-excising cassette (SEC) was removed by a 4-5 hour heat-shock of L1 larvae at 32°C. Non-Roller F1 progeny were isolated to create the strain SS1241 *lin-52(bn133(lin-52p::TagRFP-T::3xFLAG::lin-52 3' UTR)) III / hT2G [bli-4(e937) let-?(q782) qIs48] (I;III).*

To generate *lin-52(WT)*, 2 Cas9 target sites were identified near the 5' and 3' ends of the *TagRFP-T-3xFLAG* coding sequence. Single guide RNA sequences were cloned into pDD162. The *lin-52* WT homologous repair template was generated by amplifying homology arms containing the *lin-52* promoter with the gene's coding sequence and the *lin-52* 3' UTR and cloned into the C-terminal tag digested pDD282 vector. The following CRISPR/Cas9 and co-injection marker plasmid mix was microinjected into the germline of ~50 SS1241 young adults: 50 ng / µL *TagRFP-T* 5' sgRNA-Cas9 vector (pPDG21), 50 ng / µL *TagRFP-T* 3' sgRNA-Cas9 vector (pPDG22), 2.5 ng / µL pCJF90, 5 ng / µL pCFJ104, and 10 ng / µL *Plin-52::lin-52 CDS-GFP^SEC^3xFLAG::lin-52utr* (pPDG17). CRISPR/Cas9-positive progeny were treated with hygromycin and screened for the Roller phenotype and absence of fluorescent co-injection marker expression. Individuals from 2 of 3 positive selection plates were selected and made homozygous to create strains SS1325 and SS1326 *lin-52(bn138(lin-52::GFP^SEC^3xFLAG)) III*. The SEC was removed by heat-shock, and non-Roller F1 progeny were isolated to create the strains SS1256 and SS1257 *lin-52(bn139(lin-52::GFP::3xFLAG)) III*. SS1256 was backcrossed 6 times to generate strain SS1272, which was used in downstream experiments.

To generate *lin-52(1A)* and *lin-52(3A)*, 1 Cas9 target site was identified near the LxCxE coding sequence and cloned into the pDD162 vector. Single strand DNA templates included at least 40 base pairs of homology flanking the LxCxE coding sequence and silent mutations to aid in genotyping, as illustrated in Figure 2B. The following/Cas9 and co-injection marker plasmid mix was microinjected into the germline of 6 (for 1A) and 10 (for 3A) SS1256 young adults: 40 ng / µL *lin-52* LxCxE sgRNA-

Cas9 vector (pPDG59), 2.5 ng / µL pCJF90, 5 ng / µL pCFJ104, 20 ng / µL *lin-52* mutagenesis ssDNA template (1A or 3A), 40 ng / µL *dpy-10(cn64)* sgRNA (pJA58, Addgene plasmid #59933), and *dpy-10(cn64)* ssDNA template. *dpy-10(cn64)* guide and ssDNA template were co-injected to select for positive CRISPR activity in injectant progeny. Injected adults were cloned onto individual plates, and F1 progeny were screened for presence of a Roller (Rol) and/or Dumpy (Dpy) phenotype. Individual Rol and/or Dpy progeny were genotyped, resulting in 3 independent *lin-52(1A*) and 2 independent *lin-52(3A)* strains. Each strain was backcrossed 6 times to create SS1273-SS1275 *lin-52(bn150(lin-52[C44A]::GFP::3xFLAG)) III,* and SS1276 and SS1277 *lin-52(bn151(lin-52[L42A,C44A,E46A]::GFP::3xFLAG)) III*. SS1273 and SS1276 were used in downstream experiments.

Immunoblotting and co-immunoprecipitation (coIP)

CoIP lysates were prepared by grinding frozen embryos using a mortar and pestle, resuspending in lysis buffer (25 mM HEPES pH 7.6, 150 mM NaCl, 1mM DTT, 1mM EDTA, 0.5 mM EGTA, 0.1% Nonidet P-40, 10% glycerol) with Complete EDTA-free Protease Inhibitors (Roche), and sonicating twice for 30 seconds. Lysates were clarified and precleared using a mix of Protein A and Protein G Dynabeads (ThermoFisher). Protein concentrations of coIP lysates were determined using a Qubit fluorometer (ThermoFisher). For each IP, 5 µg of anti-FLAG was crosslinked to Protein G Dynabeads and 2 µg of anti-GFP or anti-LIN-35 was crosslinked to Protein A Dynabeads using dimethyl pimelimidate in 0.2 M trimethylamine pH 8.2. Crosslinking was stopped using 0.1M Tris pH 8.0, and beads were washed with 0.1 M glycine pH 2.8 before being stored in phosphate buffered saline pH 7.2 with 0.05% Tween-20. Each IP

was washed with lysis buffer, and eluted with 50 µL 2x SDS gel-loading buffer for 5 minutes at 98°C

Chromatin immunoprecipitation (ChIP) and sequential ChIP

For ChIP, chromatin extracts were precleared with Protein A Dynabeads. ChIPs were performed with 2 mg of extract and 1 µg of antibody, with 2% of the extract set aside for an input reference control. ChIPs were incubated overnight at 4°C with 1% sarkosyl. Protein A Dynabeads equilibrated in 20 µL FA buffer were added and incubated for 2 hours at 4°C. ChIPs were washed with the following buffers: once with FA buffer containing 1 M NaCl, once with FA buffer containing 0.5 M NaCl, once with TEL buffer (10 mM Tris-HCl pH 8.0, 0.25 M LiCl, 1% NP-40, 1% sodium deoxycholate, 1 mM EDTA), and twice with TE buffer (10 mM Tris-HCl pH 8.0 and 1 mM EDTA). 2 elutions of 50 µL elution buffer containing TE plus 1% SDS and 250 mM NaCl were incubated at 55°C. Eluted ChIP and input samples were incubated with proteinase K for 1 hour at 55°C. Crosslinks were reversed overnight at 65°C. DNA was purified by phenol-chloroform extraction and ethanol precipitation using glycogen as a carrier.

For sequential ChIP, chromatin extracts were precleared with Protein G Dynabeads and 4 parallel ChIPs per replicate were performed with 2.5 mg of extract and 2.5 µg of anti-FLAG antibody, with 2% of the extract set aside for an input reference control. ChIPs were incubated overnight at 4°C with 1% sarkosyl. Protein G Dynabeads equilibrated in 20 µL FA buffer were added and incubated for 2 hours at 4°C. ChIPs for each replicate were washed as described above and pooled. 2 elutions of 50 µL 0.1M $NaHCO_3$ plus 1% SDS were incubated at 55°C for 15 minutes. Elutions were divided, diluted with FA buffer with 1% sarkosyl, and incubated with anti-LIN-35 or IgG as a

negative control, with 10% of the elution set aside as a reference control. The 2nd ChIP was incubated overnight at 4°C. Protein A Dynabeads equilibrated in 20 µL FA buffer were added and incubated for 2 hours at 4°C. ChIPs were washed and eluted twice with 50 µL elution buffer with incubation at 55°C. Eluted ChIP, reference, and input samples were incubated with proteinase K for 1 hour at 55°C. Crosslinks were reversed overnight at 65°C. DNA was purified by phenol-chloroform extraction and ethanol precipitation using glycogen as a carrier.

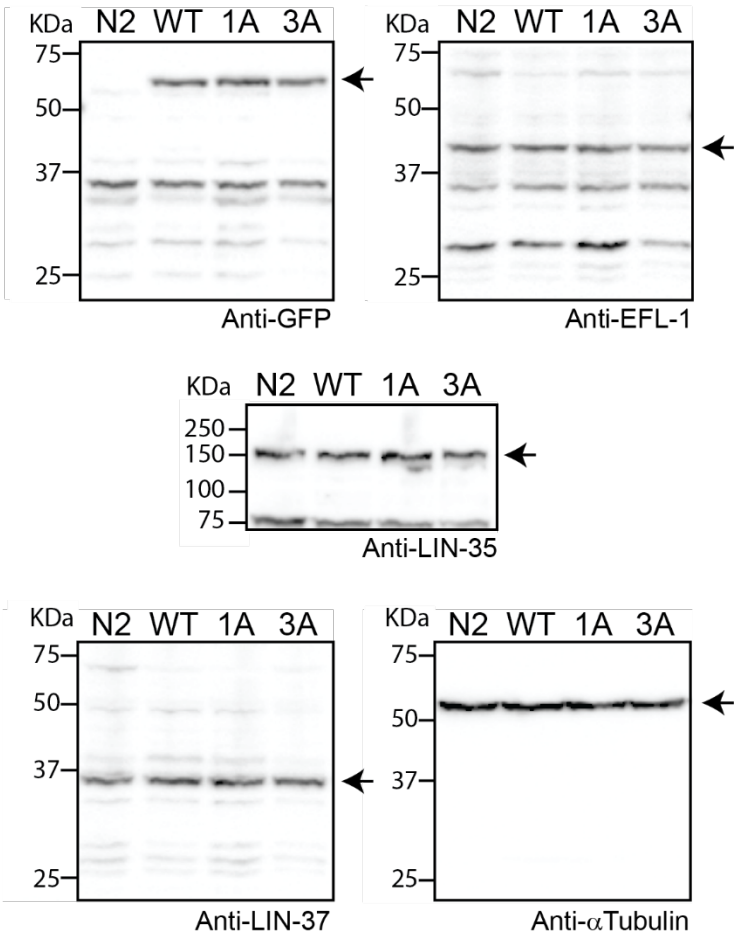

Figure S1

Full western blots of DREAM subunits LIN-52 (via GFP tag), EFL-1, LIN-35, and LIN-37 using whole worm lysates from Bristol (N2), *lin-52(WT), lin-52(1A),* and *lin-52(3A)* separated by SDS/PAGE. Antibodies used are indicated below each blot. Alpha-tubulin was used as a loading control. Membranes were cut at the 75 kDa band. Arrows indicate blot regions presented in Figure 2D.

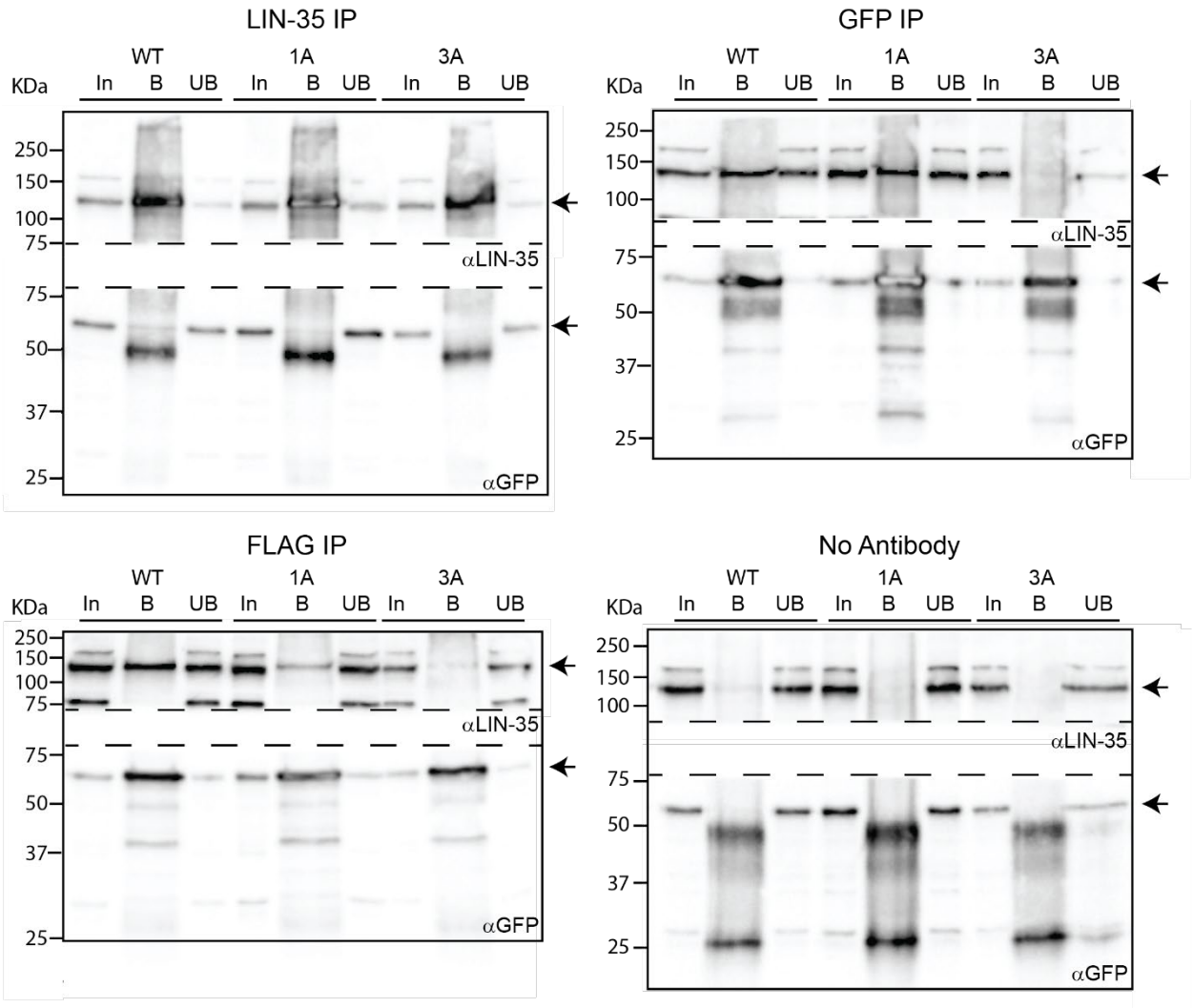

Figure S2

Full western blots of late embryo extracts from *lin-52(WT)*, *lin-52(1A)*, and *lin-52(3A)* that were immunoprecipitated with anti-LIN-35, anti-GFP, and anti-FLAG antibodies, with no antibody serving as a negative control. Proteins bound (B) and unbound (UB) were separated by SDS/PAGE and transferred to PVDF membranes that were cut at the 75 kDa band (indicated by dashed line). Antibodies used are indicated below each blot. 5% of Input (In) was included. Arrows indicate blot regions presented in Figure 3B.

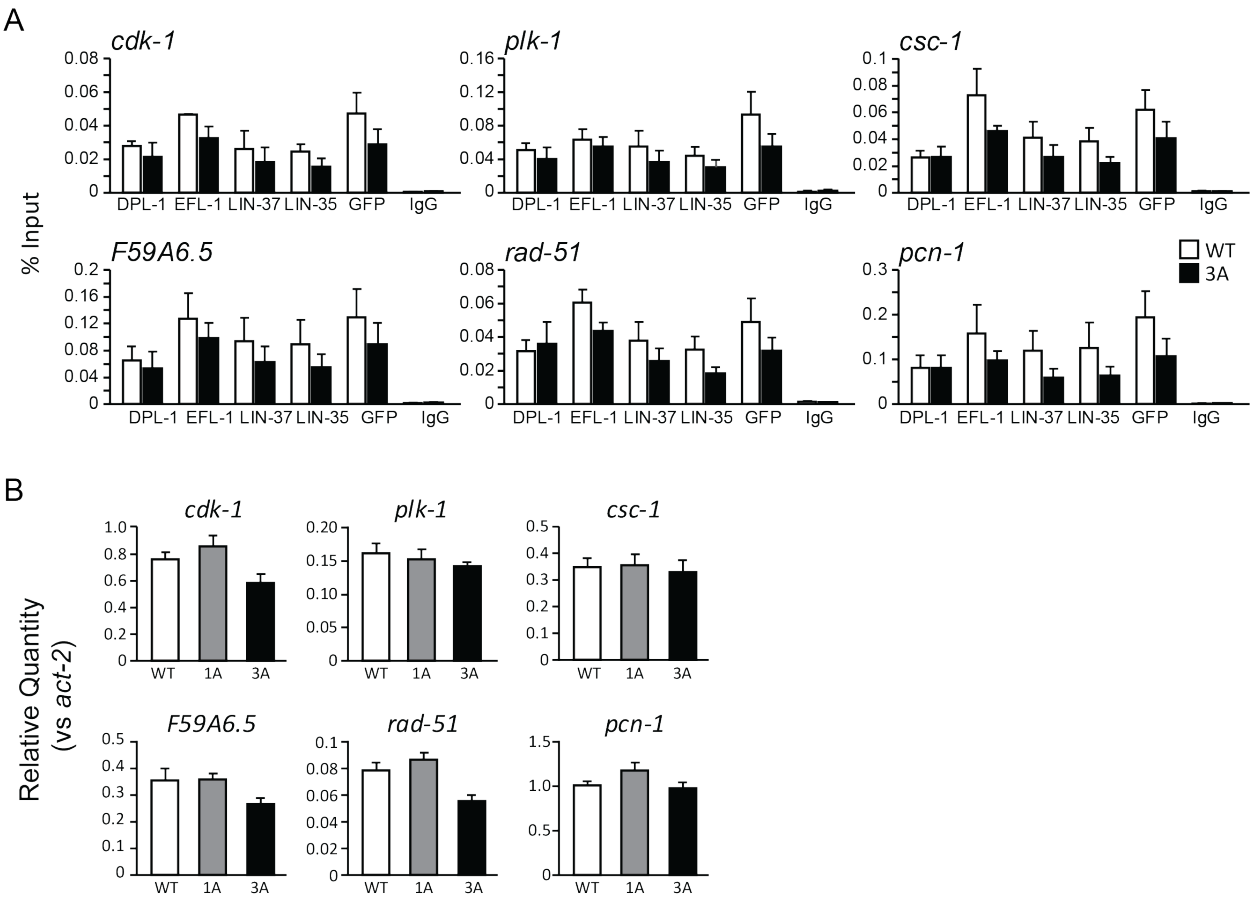

Figure S3

(A) ChIP-qPCR of 5 DREAM subunits DPL-1, EFL-1, LIN-37, LIN-35, and LIN-52 (via GFP tag) from *lin-52(WT*) (white) and *lin-52(3A*) (black) late embryo extracts at 6 DREAM target genes. IgG was used as a negative control. Signals are presented as percentage of Input DNA. Error bars indicate standard error of the mean.

(B) RT-qPCR analysis comparing transcript levels of the 6 DREAM target genes in *lin-52(WT)* (white) *lin-52(1A)* (grey), and *lin-52(3A)* (black) late embryos. Expression values from 2 independent experiments each consisting of 4 biological replicates were averaged and are presented as the relative quantity (Rq) compared to *act-2.* Error bars indicate standard error of the mean

Table S1

Name	Sequence	Notes
Cloning Primers		
lin-52 gRNA 5' F	GTCGTATCCAATAAATCCTAGGTTTTAGAG CTAGAAATAGCAAGTTA	For pPDG14
lin-52 gRNA 5' R	CTAGGATTTATTGGATACGACAAACATTTAG ATTTGCAATTCAATTATATAG	For pPDG14
lin-52 gRNA 3' F	GAAGCCAGTGAATTGAATAGGTTTTAGAGC TAGAAATAGCAAGTTA	For pPDG18
lin-52 gRNA 3' R	CTATTCAATTCACTGGCTTCAAACATTTAGA TTTGCAATTCAATTATATAG	For pPDG18
lin-52_primer1_RFP	GTCACGACGTTGTAAAACGACGGCCAGTC GCATTCGAGCAAACCGGAGGA	For pPDG13
lin-52_primer2_RFP_Nterm	CTTGATGAGCTCCTCTCCCTTGGAGACCAT TTTTTTCCTGAAATTACCGCTATATGTC	For pPDG13
lin-52_primer3	CGTGATTACAAGGATGACGATGACAAGAGA ATTGAATAGTGGTCTATCAAAAAATAATG	For pPDG13 and pPDG17
lin-52_primer4_N-term	TCACACAGGAAACAGCTATGACCATGTTAT CACCTTGGGTACTTGCTGGAT	For pPDG13
lin-52_primer1_GFP	ACGTTGTAAAACGACGGCCAGTCGCCGGC ACATTCGAGCAAACCGGAGGA	For pPDG17
lin-52_primer2_C-term	CATCGATGCTCCTGAGGCTCCCGATGCTCC CTGGCTTCCTGTCGTTTCTTC	For pPDG17
lin-52_primer4_C-term	GGAAACAGCTATGACCATGTTATCGATTTC CACCTTGGGTACTTGCTGGAT	For pPDG17
sgRNA SDM R	CAAGACATCTCGCAATAGG	Reverse primer for Q5 targeted mutagenesis, see Dickinson et al, 2013
tagRFP-sgRNA SDM 5' F	TGGCTTTCCCTCTCCCTCGGGTTTTAGAGC TAGAAATAGCAAGT	For pPDG21
tagRFP-sgRNA SDM 3' F	TGTGTCCGAGCTTGGATGGGGTTTTAGAGC TAGAAATAGCAAGT	For pPDG22
lin-52 LxCxE sgRNA SDM F	ACTTTCTTCTGGCATTGTTTGTTTTAGAGCT AGAAATAGCAAGT	For pPDG59
ChIP-qPCR Primers		
set-21 Pro F	ACGACGGGCCCAAAAGTAAA	
set-21 Pro R	TGTTGTTTCGTTTTCGCGAATTT	
mis-12 Pro F	TTCCCGACAATTCGCTCTCC	
mis-12 Pro R	CGTGTATGCACACCTCACCT	
polh-1 Pro F	TCAATGTTTGAAACCCCGCC	
polh-1 Pro R	ATACTCAGCCAAGCAGCCAA	
air-1 Pro F	ATTCGCAACGTGTCAGCAAC	
air-1 Pro R	ATGAATTTTGCTTGGCGGGT	
cdk-1 Pro F	ACAATCCTTCTCAGCGCGT	
cdk-1 Pro R	CGATAGAAAAGGCGTAAGCGTG	
plk-1 Pro F	CGCTGTTTTGTTTAGCACCCT	
plk-1 Pro R	CAAGAGGCGAGCTGGAAACT	
csc-1 Pro F	TTTCCTTCTTTTGCGCGTGG	
csc-1 Pro R	CGGAGAAAATCGAATTTTTGAGGG	
F59A6.5 Pro F	GAAAACGGGTTCCGTATGCT	
F59A6.5 Pro R	TCTCTCTTCCGCAAACACCG	

rad-51 Pro F	GCGCACTTGCTGTACTCTTG	
rad-51 Pro R	CCGTTCCTATCGGTGCCTTT	
pcn-1 Pro F	TGAACGGAGAAAGTGCGATGA	
pcn-1 Pro F	GTTGCGCGTCAAATAAAATGCC	
RT-qPCR primers		
set-21 1359-1524 F	AAATGTTGCGCGAACTGTCG	
set-21 1359-1524 R	GTCCGTGTACGTCTTTCCGT	
mis-12 370-515 F	ATTCGACAGCTCCGCATCAA	
mis-12 370-515 R	ATTCGTGTTGGGCTATCGGG	
polh-1 759-842 F	TGTTCGAGGATTTGGCGGAA	
polh-1 759-842 R	TCCACTTCGAGCAGTTCACC	
air-1 594-740 F	ACGCCATACATTGTGCGGTA	
air-1 594-740 R	CCAGTTTGATTGGCGAACGG	
cdk-1 703-911 F	TTCAGAGTTCTCGGCACACC	
cdk-1 703-911 R	TTCGCGTTGAGACGAAGTGA	
plk-1 1050-1280 F	GAACAATGCCGATCGTGAGC	
plk-1 1050-1280 R	CCGATGCCATACTTGTCCGA	
csc-1 425-588 F	TTCCGATTGCTCCATCTGGC	
csc-1 425-588 R	CGAGAAGGCGATTTCCTCGT	
F59A6.5 (1964-2136) F	GCCAGATTGATGCGAAGCAG	
F59A6.5 (1964-2136) R	TTGACGTCTTTTCTCCGCGA	
rad-51 (534-686) F	CAATGCCACTTTTCGACCCG	
rad-51 (534-686) R	TCGGACATCATTGCTCCTGC	
pcn-1 (151-386) F	AAGTTGGAGGTCGGCCTTTT	
pcn-1 (151-386) R	ATCCCGAGATGTTCGCTGTC	